Available online at www.sciencedirect.com
SCIENCE DIRECT®
Icarus 170 (2004) 295–311
ICARUS
www.elsevier.com/locate/icarus

# Bias-corrected population, size distribution, and impact hazard for the near-Earth objects ☆

Joseph Scott Stuart [a,*], Richard P. Binzel [b]

[a] *MIT Lincoln Laboratory, S4-267, 244 Wood Street, Lexington, MA 02420-9108, USA*
[b] *MIT EAPS, 54-426, 77 Massachusetts Avenue, Cambridge, MA 02139, USA*

Received 20 November 2003; revised 2 March 2004

Available online 11 June 2004

**Abstract**

Utilizing the largest available data sets for the observed taxonomic (Binzel et al., 2004, Icarus 170, 259–294) and albedo (Delbo et al., 2003, Icarus 166, 116–130) distributions of the near-Earth object population, we model the bias-corrected population. Diameter-limited fractional abundances of the taxonomic complexes are A-0.2%; C-10%, D-17%, O-0.5%, Q-14%, R-0.1%, S-22%, U-0.4%, V-1%, X-34%. In a diameter-limited sample, $\sim 30\%$ of the NEO population has jovian Tisserand parameter less than 3, where the D-types and X-types dominate. The large contribution from the X-types is surprising and highlights the need to better understand this group with more albedo measurements. Combining the C, D, and X complexes into a "dark" group and the others into a "bright" group yields a debiased dark-to-bright ratio of $\sim 1.6$. Overall, the bias-corrected mean albedo for the NEO population is $0.14 \pm 0.02$, for which an $H$ magnitude of $17.8 \pm 0.1$ translates to a diameter of 1 km, in close agreement with Morbidelli et al. (2002, Icarus 158 (2), 329–342). Coupling this bias corrected taxonomic and albedo model with the $H$ magnitude dependent size distribution of (Stuart, 2001, Science 294, 1691–1693) yields a diameter distribution with $1090 \pm 180$ NEOs with diameters larger than 1 km. As of 2004 June, the Spaceguard Survey has discovered 56% of the NEOs larger than 1 km. Using our size distribution model, and orbital distribution of (Stuart, 2001, Science 294, 1691–1693) we calculate the frequency of impacts into the Earth and the Moon. Globally destructive collisions ($\sim 10^{21}$ J) of asteroids 1 km or larger strike the Earth once every $0.60 \pm 0.1$ Myr on average. Regionally destructive collisions with impact energy greater than $4 \times 10^{18}$ J ($\sim 200$ m diameter) strike the Earth every $56{,}000 \pm 6000$ yr. Collisions in the range of the Tunguska event ($4–8 \times 10^{16}$ J) occur every 2000–3000 yr. These values represent the average time between randomly spaced impacts; actual impacts could occur more or less closely spaced solely by chance. As a verification of these impact rates, the crater production function of Shoemaker et al. (1990, Geological Society of American Special Paper 247) has been updated by combining this new population model with a crater formation model to find that the observed crater production function on both the Earth and Moon agrees with the rate of crater production expected from the current population of NEOs.


*Keywords:* Asteroids; Cratering; Moon

## 1. Introduction

Several pieces must be brought together to understand the near-Earth objects (NEOs). Four of the pieces that can be readily described are (i) the taxonomic distribution as measured by observational sampling, (ii) albedos that can be associated with the taxonomic categories, (iii) observed orbital distributions and number of objects as determined from discovery statistics, and (iv) debiasing of the discovery statistics and observational sampling using the taxonomic and albedo information. This first piece is discussed in a companion paper (Binzel et al., 2004) which discusses the taxonomic distribution of the NEOs from visible and near-infrared reflectance spectroscopy. A complementary program of thermal infrared measurements to determine albedos supplies the second piece and is detailed in Delbo et al. (2003). For the third piece, the most extensive set of NEO discovery statistics are provided by the LINEAR survey (Stokes et al., 2000; Stuart, 2001). This work brings the fourth piece, a debiasing of the discovery statistics using the taxonomic and albedo information.

Recent estimates of the number of NEOs constrain the size of the population as a function of absolute magnitude

☆ This paper to appear in print with manuscript #I08787.

* Corresponding author. Fax: 781-981-0991.
*E-mail address:* stuart@ll.mit.edu (J.S. Stuart).

0019-1035/$ – see front matter 
doi:10.1016/j.icarus.2004.03.018

(Bottke et al., 2000, 2002; Stuart, 2001). The reflectivity, or geometric albedo (Russell, 1916) must be known to estimate the size of an NEO from its measured absolute magnitude (e.g., Harris and Harris, 1997; Fowler and Chillemi, 1992). Since few albedo measurements have been made for NEOs, the absolute magnitudes cannot be converted to physical sizes. Albedo measurements are available for fewer than 1% of the NEOs, and those albedo values span a wide range, from 0.023 to 0.63 (Binzel et al., 2002a, 2002b). This factor of 27 variation in albedo corresponds to more than a factor of 5 range in possible diameter of an NEO with a given absolute magnitude. Furthermore, observational selection effects tend to bias the discovered and observed population of NEOs toward high albedo objects, and high albedo taxonomic classes. Therefore, the number of NEOs as a function of diameter is poorly known.

Several past attempts have been made to debias the albedo and taxonomic distributions of the NEOs. Luu and Jewitt (1989) used a Monte Carlo simulation of NEO discoveries to estimate the observational bias in the ratio of an assumed bimodal population of light (S-type, albedo = 0.15) and dark (C-type, albedo = 0.047) NEOs. Shoemaker et al. (1990) used a similar argument to obtain a mean albedo for the NEOs and to convert their absolute magnitude distribution to a diameter distribution (and ultimately to distributions for impact energy and crater diameter). The primary reason for updating these earlier estimates here is to make use of the order-of-magnitude increase in the number of known, cataloged NEOs, to take account of the capabilities of current NEO search programs that lead to observational biases that are different from those of the search programs of the 1980s, and to include the latest taxonomic classifications and albedo measurements for NEOs.

Morbidelli et al. (2002) have recently conducted a similar study. They attempt to define a reasonable albedo distribution for each of the main-belt source regions that their earlier work (Bottke et al., 2000, 2002) identified as being the most important suppliers of asteroidal and cometary material to the NEO population. The albedo distributions of the main-belt source regions were then combined in the correct proportions to yield an albedo distribution of the NEOs. Unfortunately, the albedo distribution of the main-belt source regions is poorly known for asteroids in the same size range as the NEOs. Thus, the albedos of the small members of the main-belt source regions that ultimately become the NEOs must be extrapolated from the albedos of the larger members. The work presented here is a complementary approach that uses direct observation of the physical properties of a subset of the NEOs to determine the albedo distribution of the NEOs for which albedos are not available.

This paper describes the debiasing of the NEO taxonomy and albedo data in a two-step process. First, the absolute magnitude and orbital element distributions from Stuart (2001) are combined with albedo measurements (from Delbo et al., 2003) within each taxonomic complex to define an average albedo for each complex. Second, the average albedos for the complexes are combined with the observed fractional abundances of the complexes to produce debiased, or diameter-limited fractional abundances for each complex. The average albedos and debiased fractional abundances of the complexes are combined to derive an overall average albedo and a diameter distribution for the NEOs.

A new model of the diameter distribution of the NEOs warrants a new analysis of the impact threat to the Earth. The distributions of NEO orbital elements from Stuart (2001) are combined with Öpik-type calculations to determine average impact probabilities. The impact probabilities are combined with the diameter distribution of the NEOs to evaluate the flux of large NEOs into the Earth and Moon. Several crater scaling laws are then used to compare the expected rate of crater production on the Earth and on the Moon to the observed cratering record.

### 1.1. Trends in albedo and taxonomy

The first step in debiasing the albedo distribution of the NEOs is to determine whether the albedo is correlated with the sizes or orbital parameters of the NEOs. There are suggestions that the albedos of S-type asteroids increase with decreasing size when main-belt asteroids are combined with NEOs (Binzel et al., 2002b, 2004; Delbo et al., 2003). Analyzing just the NEOs, we find that the correlation between albedo and absolute magnitude is not statistically significant at the 95% level. For the purposes of the present analysis which focuses only on the NEOs, we assume that there is no correlation between albedo and absolute magnitude. Similarly, we do not attempt to model any correlation between taxonomic class and absolute magnitude.

In our sample, there is no statistically significant correlation between albedo and orbital eccentricity or inclination. There is perhaps some correlation between albedo and semimajor axis. This correlation is better explained as a dependence of albedo on the jovian Tisserand parameter (Fernández et al., 2001; Binzel et al., 2004). The jovian Tisserand parameter may be calculated as $T_J = a_J/a + 2\cos(i)\sqrt{(a/a_J)(1-e^2)}$ (Kresák, 1979), where $a_J$ is the semimajor axis of Jupiter, and $a$, $e$, and $i$, are the semimajor axis, eccentricity, and inclination of the asteroid. $T_J$ is approximately equal to the Jacobi integral, a conserved quantity in the circular, restricted, three-body problem, and has traditionally been used to classify comet populations (e.g., Weissman et al., 2002).

As with the albedos, the relative abundances of the taxonomic complexes show some correlations with orbital parameters. As shown in Fig. 5 of Binzel et al. (2004) the trend is best explained as a correlation with the jovian Tisserand parameter. Even before debiasing, the darker complexes (C, D, and X) are more abundant than the bright complexes (S and Q) for $T_J \leqslant 3$. There do not appear to be any other significant trends in the relative abundances of the major taxonomic complexes versus the orbital parameters.

Table 1
NEO spectral and albedo data

| Taxonomic complex | Includes | # of NEO albedos | # of NEO spectra |
|---|---|---|---|
| A | A | 0 | 1 |
| C | C, C-subgroups, B, F, G | 6 | 23 |
| D | D, T | 1 | 9 |
| O | O | 1 | 6 |
| Q | Q, Sq | 7 | 80 |
| R | R | 0 | 1 |
| S | S, K, L, S-subgroups | 12 | 125 |
| U | U | 0 | 3 |
| V | V | 3 | 14 |
| X | X, X-subgroups, E, M, P | 6 | 48 |
| Totals | | 36 | 310 |

The taxonomic classes of Bus and Binzel (2002b) are grouped into 10 complexes following Binzel et al. (2004). The number of NEO spectra and NEATM albedos (Delbo et al., 2003) available for each complex is given.

To debias the NEO albedo and taxonomic distributions, we will therefore divide the NEO population into two groups defined by $T_J > 3$ and $T_J \leqslant 3$. Chapter 4 of Stuart (2003) contains additional figures and analysis of the correlations between albedo, taxonomy, orbital parameters, and size to support the conclusion drawn here that $T_J$ is the most important parameter that controls trends in the taxonomy data. An analysis presented in Chapter 4 of Stuart (2003) investigates what happens if $T_J$ is not used to divide the NEO population. That analysis is found to significantly underestimate the number of low albedo objects, particularly in the D complex.

### 1.2. Spectroscopic and albedo data

The taxonomic and albedo data used in this analysis are summarized in Tables 1 and 2. The visible-wavelength spectral taxonomy is described in Binzel et al. (2004) and Bus and Binzel et al. (2002a; 2002b). The albedo data are described in Delbo et al. (2003) and Harris and Lagerros (2002). Here we follow the delineations of the complexes given by Bus (1999) with the actual groupings taken from the assignments made in Table 2 of Binzel et al. (2004).

### 1.3. Absolute magnitude and diameter distributions

Before proceeding to a discussion of the methods used to debias the albedo and spectral data, we will first explain several equations necessary for working with population distribution functions based upon absolute magnitude or diameter. The conversion between absolute magnitude and diameter is (Harris and Harris, 1997):

$$H = C - 5\log_{10} D - 2.5\log_{10} p_V, \tag{1}$$

where $C = 15.618$ is a constant that defines the absolute magnitude system.

The population model of Stuart (2001) fits an exponential distribution to the number of NEOs versus absolute magnitude of the following form:

$$N(< H) = B10^{\beta H}, \tag{2}$$

where the exponent is $\beta = 0.39 \pm 0.013$. Equation (2) gives the cumulative number of NEOs with absolute magnitudes less than (i.e., brighter than) a specified value. That equation assumes that the population can be approximated by a simple exponential function. The number of NEOs can be expressed equivalently as a diameter distribution, or the cumulative number of NEOs with diameters greater than a specified value:

$$N(> D) = AD^{-\alpha}. \tag{3}$$

Using Eq. (1), the exponential slope of the absolute magnitude distribution, $\beta$, can be converted into the power-law slope of the diameter distribution quite simply as $\alpha = 5\beta$. Likewise, the scaling constants, $A$, and $B$, can be related by $A = Bp_V^{-2.5\beta}10^{\beta C}$, where $p_V$ is the visual geometric albedo.

We now assume that the NEOs can be divided into $M$ taxonomic complexes where all the members of a complex, $i$, have the same albedo, $p_i$, and the population distribution of each taxonomic complex follows Eqs. (2) and (3). For each complex we may write that the number of NEOs of that type with absolute magnitudes brighter than $H$, is given by

$$N_i(< H) = f_i N(< H) = f_i B10^{\beta H}, \tag{4}$$

where the $f_i$ are the magnitude-limited fractional abundances of each complex, and $\sum_{i=1}^{M} f_i = 1$. These magnitude-limited fractional abundances are the proportions of the NEOs that would fall into each of the taxonomic complexes if one were to classify all of the NEOs up to some limiting absolute magnitude. The population in each complex can also be described by a diameter distribution given by

$$N_i(> D) = g_i N(> D) = g_i AD^{-\alpha}, \tag{5}$$

where the $g_i$ are the diameter-limited fractional abundances of each complex, and $\sum_{i=1}^{M} g_i = 1$. These diameter-limited fractional abundances are the proportions of the NEOs that would fall into each of the taxonomic complexes if one were to classify all of the NEOs down to some limiting diameter. The $f_i$ differ from the $g_i$ because the members of one complex have a different albedo from the members of the other

Table 2
Details of NEATM albedo measurements used here

| Name | Complex | Absolute magnitude | Albedo | Albedo reference |
|---|---|---|---|---|
| (433) Eros | S | 11.2 | 0.21 | 1 |
| (1566) Icarus | Q | 16.0 | 0.33 | 2 |
| (1580) Betulia | C | 14.6 | 0.17 | 2 |
| (1627) Ivar | S | 12.9 | 0.15 | 3 |
| (1862) Apollo | Q | 16.3 | 0.26 | 4, 2 |
| (1866) Sisyphus | S | 13.0 | 0.15 | 3 |
| (1915) Quetzalcoatl | S | 19.0 | 0.31 | 2 |
| (1980) Tezcatlipoca | S | 14.0 | 0.14 | 1, 2 |
| (2100) Ra-Shalom | C | 16.1 | 0.082 | 3 |
| (2201) Oljato | Q | 16.9 | 0.24 | 2 |
| (3200) Phaethon | C | 14.5 | 0.11 | 4, 2 |
| (3551) Verenia | V | 16.8 | 0.53 | 2 |
| (3554) Amun | M | 15.9 | 0.17 | 4, 2 |
| (3671) Dionysus | C | 16.7 | 0.16 | 2 |
| (3757) 1982 XB | S | 19.0 | 0.34 | 2 |
| (4034) 1986 PA | O | 18.2 | 0.52 | 3 |
| (4055) Magellan | V | 14.9 | 0.31 | 3 |
| (4660) Nereus | E | 18.7 | 0.55 | 3 |
| (5587) 1990 SB | Q | 14.1 | 0.32 | 3 |
| (5604) 1992 FE | V | 17.7 | 0.48 | 3 |
| (5751) Zao | E | 14.9 | 0.36 | 3 |
| (6053) 1993 BW3 | Q | 15.2 | 0.18 | 5, 2 |
| (6178) 1986 DA | M | 15.1 | 0.14 | 4, 2 |
| (6489) Golevka | Q | 19.1 | 0.63 | 6, 2 |
| (9856) 1991 EE | S | 17.0 | 0.30 | 7 |
| (14402) 1991 DB | C | 18.9 | 0.14 | 3 |
| (16834) 1997 WU22 | S | 15.9 | 0.22 | 3 |
| (19356) 1997 GH3 | S | 17.0 | 0.34 | 3 |
| (25330) 1999 KV4 | C | 16.3 | 0.052 | 3 |
| 1999 FK21 | S | 18.0 | 0.32 | 3 |
| 1999 NC43 | Q | 16.1 | 0.14 | 3 |
| 2000 BG19 | P | 17.8 | 0.043 | 3 |
| 2000 PG3 | D | 15.7 | 0.042 | 3 |
| 2001 FY | S | 18.8 | 0.52 | 3 |
| 2002 BM26 | P | 20.1 | 0.023 | 3 |
| 2002 CT46 | S | 20.8 | 0.32 | 3 |

Shown are the MPC catalog number (if the asteroid is numbered) and name or provisional designation along with the taxonomic complex from the Bus Taxonomy, the V-band absolute magnitude, the V-band albedo from the NEATM thermal model, and the publication from which the albedo was obtained. The reference numbers correspond to the following papers: 1—Harris and Davies (1999); 2—Harris and Lagerros (2002); 3—Delbo et al. (2003); 4—Harris (1998); 5—Pravec et al. (1997); 6—Mottola et al. (1997); 7—Harris et al. (1998). The final published versions of these albedo measurements differed slightly from the pre-publication results given in Table 4.2 of Stuart (2003) and used in the analysis there. Because of these slight changes in the albedo values, there are slight differences between the results in this paper and in Stuart (2003). These results take precedence.

complexes and the number of objects increases rapidly with decreasing size. The $f_i$ and $g_i$ can be related by the following equations:

$$g_i = \frac{f_i p_i^{-2.5\beta}}{\sum_{j=1}^{M} f_j p_j^{-2.5\beta}}, \tag{6}$$

$$f_i = \frac{g_i p_i^{2.5\beta}}{\sum_{j=1}^{M} g_j p_j^{2.5\beta}}. \tag{7}$$

We are now in a position to define an average albedo for all the NEOs, averaging over all of the $M$ taxonomic complexes. We start with the definition that we want an average albedo, $p_N$ such that when Eq. (1) is used, $N(>D) = N(<H)$ for all diameters and absolute magnitudes. This "number-averaged" albedo is slightly different from the geometric mean which is usually used to average together albedos from different objects. The number-averaged albedo assures that the number of NEOs brighter than a given absolute magnitude is equal to the number with diameters larger than the equivalent diameter when the number-averaged albedo is used in Eq. (1) to convert between absolute magnitude and diameter. The number-averaged albedo may be calculated from the albedos of each complex and either the magnitude-limited fractional abundances or the diameter-limited fractional abundances as follows:

$$p_N = \left( \sum_{i=1}^{M} f_i p_i^{-2.5\beta} \right)^{1/(-2.5\beta)}, \tag{8}$$

$$p_N = \left( \sum_{i=1}^{M} g_i p_i^{2.5\beta} \right)^{1/(2.5\beta)}. \tag{9}$$

If Eqs. (6) and (7) are used to relate $f_i$ and $g_i$, then Eqs. (8) and (9) give identical values. They are two different ways to calculate the same value of $p_N$.

If one is interested in a particular diameter, $D_o$, then one can use the average albedo, $p_N$ to define an average absolute magnitude, $H_o$, that is equivalent to $D_o$. One can calculate $H_o$ by using $p_N$ and $D_o$ in Eq. (1). This averaging function has the nice property that the same answer will be obtained if the values of $p_i$ are averaged in subgroups, and then the subgroups averaged with correct weightings, or if all are averaged as one group.

### 1.4. Magnitude-limited debiasing

In any telescope search program to discover or study asteroids, the primary observational selection effect is that the telescope is flux limited. That is, objects with bright apparent magnitudes are more likely to be observed than fainter objects. Since we are assuming that there are no correlations between the orbital parameters and the spectral properties of the NEOs, the primary selection effect is that NEOs with brighter absolute magnitudes are more likely to be discovered, and observed for spectra. Therefore, as a first step, we assume that the observed fractional abundances of NEO spectral types, and the observed albedos within a taxonomic complex are absolute magnitude-limited samples, or equivalent to the $f_i$ defined in Eq. (4). We can then use Eq. (8) to obtain debiased or diameter-limited values.

Contrary to the assumptions made above, the actual NEOs within a single taxonomic complex do not all have the same albedo. To define an average albedo within each complex we assume that each albedo measurement within a single complex represents a subset that have that albedo. We assume that the measured albedos are a magnitude-limited sample of the albedo values within a complex, and we use Eq. (8) to obtain an average albedo for each complex. It is important to debias the measured albedos when obtaining average albedos in each complex. Otherwise, the average albedos within each complex would be erroneously high when combining the complexes to obtain an overall average albedo. The resulting debiased albedos are given in Fig. 1.

Three of the taxonomic complexes have no NEO members with a measured albedo, so the A, R, and U complexes have been assigned albedos from average main-belt values.[1] These three complexes (and the O complex with only a single measured albedo) represent a tiny fraction of the NEOs and so they have very little effect on the final answer. The D complex also has only one member with a NEATM measured albedo, and there are enough D-types to significantly affect the final answer. However, the measured albedo for that D-type NEO (0.042) is quite similar to the average of main-belt D-types, so this NEOs albedo is used as the albedo for the D complex.

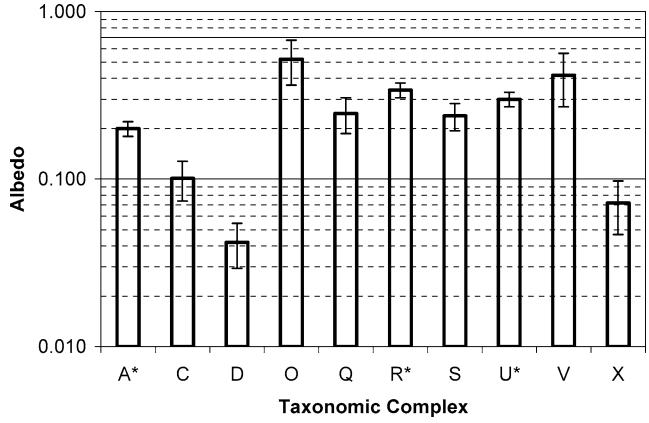


Fig. 1. Debiased average albedos. The debiased average albedo of each taxonomic complex is shown as calculated from Eq. (8) using NEATM albedos for NEOs with SMASS taxonomy classifications. Complexes marked with * have been assigned albedos from average main-belt values.

To calculate uncertainties for magnitude-limited debiasing, we assume a straightforward Gaussian model of errors and use the standard formula for propagating uncertainties (Bevington, 1969, p. 59). Each of the albedo measurements from NEATM is assigned an uncertainty of 30%. The uncertainty in the albedo is difficult to estimate precisely, because the uncertainty stems primarily from uncertainties in the thermal model used to perform the calculation rather than statistical noise in the thermal IR data. An uncertainty of 30% is perhaps larger than necessary, but is a safe limit (Delbo et al., 2003). The observed fractional abundances of each of the taxonomic complexes are assigned Poisson error bars ($\sigma_N = \sqrt{N}$). The uncertainty in the value of $B$ is taken from the linear least-squares fit to the log of the number of NEOs as a function of absolute magnitude (Stuart, 2001). All of these uncertainties are combined to calculate the one-standard-deviation uncertainty in the average albedo of the taxonomic complexes, the debiased fractional abundances of the taxonomic complexes, and the overall, average albedo of the NEOs.

Several alternative debiasing schemes were explored in Chapter 4 of Stuart (2003) involving models of the asteroid observing programs that produced the NEO orbits, taxonomies, and albedos. Those models explicitly include the effects of differential phase darkening (Luu and Jewitt, 1989). Those alternatives were all found to produce results that differed from the magnitude-limited debiasing technique by less than 1 standard deviation. The NEO population distribution of Bottke et al. (2002) was also used in place of the Stuart population distribution to test the robustness of the debiasing to differing NEO orbital parameter distributions and to a different value of the absolute magnitude slope parameter, $\beta$. Debiasing with the Bottke distribution also

[1] The average albedos for main-belt asteroids in the A, R, and U taxonomic complexes were calculated as the geometric mean of the albedos from IRAS (Tedesco et al., 2002) that have the appropriate taxonomic classification from the file Taxonomic Classifications, Version 3 in the Physical Data System Small Bodies Node (http://pdssbn.astro.umd.edu/SBNast/holdings/EAR-A-5-DDR-TAXONOMY-V3.0.html) which is a compilation of the taxonomies of Tholen (1984), Barucci et al. (1987), Tedesco et al. (1989), Howell et al. (1994), and Xu et al. (1995).

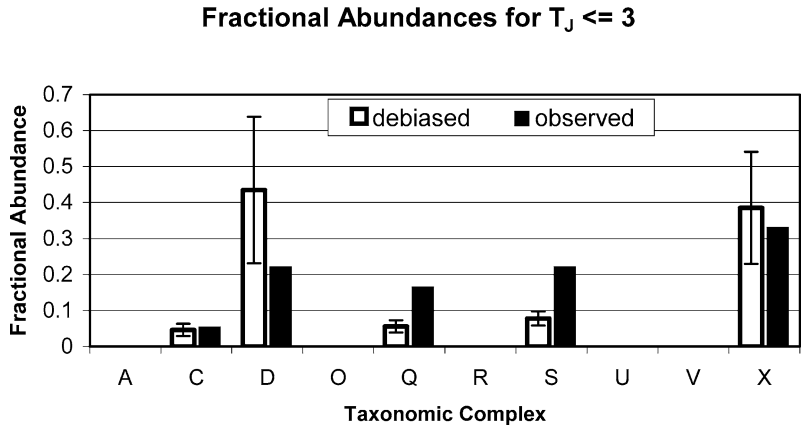


Fig. 2. Fractional abundances versus taxonomy for NEOs with jovian Tisserand parameter less than 3. The observed fractional abundances are simple counts of the $T_J \leqslant 3$ NEOs with spectra in each complex. Debiased fractional abundances of the taxonomic complexes are computed with magnitude-limited debiasing. The dark NEO complexes, particularly the D-types dominate in the $T_J \leqslant 3$ region.

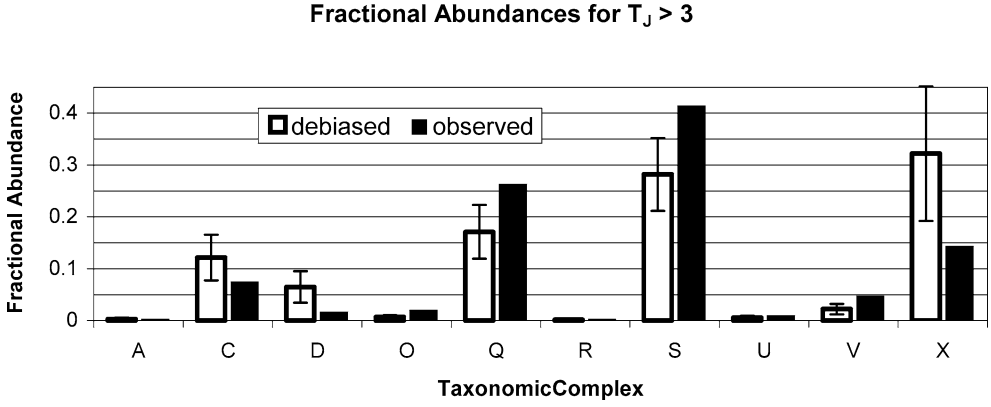


Fig. 3. Fractional abundances versus taxonomy for NEOs with jovian Tisserand parameter greater than 3. The observed fractional abundances are simple counts of the $T_J > 3$ NEOs with spectra in each complex. Debiased fractional abundances of the taxonomic complexes are computed with magnitude-limited debiasing. The bright NEO complexes (S, Q), are abundant in the $T_J > 3$ region, but there is a large contribution from the relatively dark X-types.

produced results that agree with these results as described in Stuart (2003).

### 1.5. *Results of albedo and taxonomy debiasing*

Only one NEO with $T_J \leqslant 3$ has a NEATM albedo measurement (2000 PG3), and only 7 NEOs with $T_J \leqslant 3$ have albedo values from any source (Binzel et al., 2002a, 2002b). Therefore, the average albedos for the taxonomic complexes are assumed to be the same for the $T_J \leqslant 3$ objects and the $T_J > 3$ objects. However, the fractional abundances of the taxonomic complexes are allowed to vary between the $T_J \leqslant 3$ and $T_J > 3$ groups. Figure 1 shows the debiased average albedo for each of the taxonomic complexes.

Figures 2 and 3 show the magnitude-limited and diameter-limited fractional abundances of the taxonomic complexes for the two regions. In both cases the debiasing amplifies the number of NEOs in the dark complexes and reduces the proportion of NEOs in the brighter complexes. In Fig. 4 the difference between the $T_J \leqslant 3$ and $T_J > 3$ NEOs is dramatically apparent with the $T_J \leqslant 3$ group being much more dominated by very dark objects. Table 3 lists the overall properties for the two regions. The $T_J \leqslant 3$ NEOs account for 30% of the population in a diameter-limited sample, while the $T_J > 3$ NEOs account for 70%. The final debiased fractional abundances and average albedos of the ten taxonomic complexes are given in Table 4.

### 1.6. *Diameter distribution of the NEOs*

So far, this analysis of the albedos and taxonomic categories of the NEOs has assumed that the number of NEOs is an exponential function of the absolute magnitude. The best fit for the cumulative distribution (Stuart, 2001, 2003) was found to be $N(< H) = 10^{-3.88+0.39H}$. This power law is obtained from a fit to the binned, non-cumulative absolute magnitude distribution which is not exactly a simple exponential function. Using the albedos and fractional abundances from Table 4, we convert the binned, non-cumulative absolute magnitude distribution into a diameter distribution without first simplifying it to an exponential form. This is done as follows:

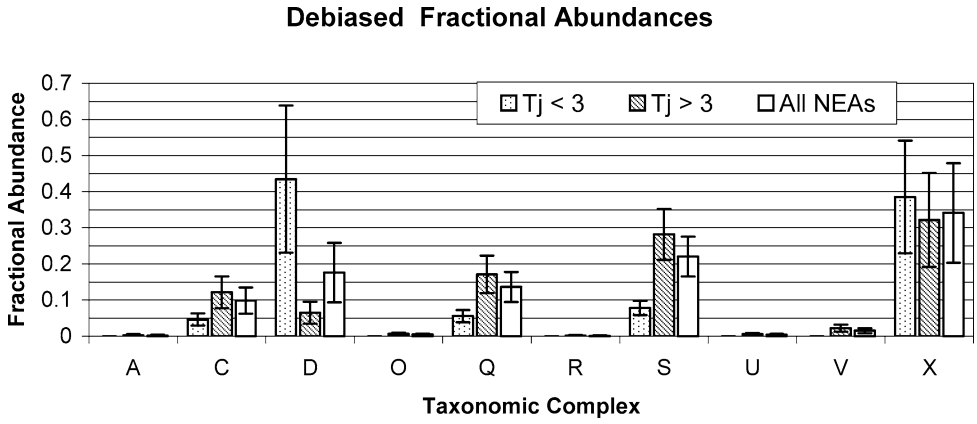


Fig. 4. Debiased, or diameter-limited, fractional abundances versus taxonomy. The NEOs are separated into groups with jovian Tisserand parameter greater than or less than 3, and shown as a whole. Overall, the S- and X-type NEOs are the most abundant. However, in the $T_J \leqslant 3$ region, the dark complexes, particularly the D-types dominate. The bars are in left–right order as indicated in the caption.

Table 3
Summary of average NEO properties for debiasing with Tisserand parameter

| | $T_J \leqslant 3$ | $T_J > 3$ | Combined |
|---|---|---|---|
| Average albedo | $0.083 \pm 0.01$ | $0.163 \pm 0.06$ | $0.139 \pm 0.02$ |
| 1 km equivalent $H$ magnitude | $18.32 \pm 0.1$ | $17.59 \pm 0.2$ | $17.76 \pm 0.1$ |
| Number bigger than 1 km | $297 \pm 50$ | $694 \pm 110$ | $991 \pm 160$ |

Average albedo, absolute magnitude equivalent to a 1 km diameter NEO, and predicted number of NEOs with diameters larger than 1 km for the NEOs with jovian Tisserand parameter greater than or less than 3 are given. This analysis assumes a simple power law model for the NEOs absolute magnitude distribution, in comparison to Fig. 5 which accounts for non-linear features of the observed absolute magnitude distribution.

Table 4
Fractional abundances and albedos

| Taxonomic complex | $T_j \leqslant 3$ fractional abundance | $T_j > 3$ fractional abundance | Total fractional abundance | Debiased albedo |
|---|---|---|---|---|
| A | $0.000 \pm 0.000$ | $0.003 \pm 0.003$ | $0.002 \pm 0.002$ | $0.200 \pm 0.020$ |
| C | $0.046 \pm 0.016$ | $0.120 \pm 0.041$ | $0.098 \pm 0.033$ | $0.101 \pm 0.027$ |
| D | $0.433 \pm 0.194$ | $0.064 \pm 0.029$ | $0.175 \pm 0.078$ | $0.042 \pm 0.013$ |
| O | $0.000 \pm 0.000$ | $0.007 \pm 0.003$ | $0.005 \pm 0.002$ | $0.520 \pm 0.156$ |
| Q | $0.058 \pm 0.016$ | $0.176 \pm 0.049$ | $0.141 \pm 0.039$ | $0.247 \pm 0.060$ |
| R | $0.000 \pm 0.000$ | $0.002 \pm 0.002$ | $0.001 \pm 0.001$ | $0.340 \pm 0.034$ |
| S | $0.080 \pm 0.018$ | $0.285 \pm 0.066$ | $0.224 \pm 0.051$ | $0.239 \pm 0.044$ |
| U | $0.000 \pm 0.000$ | $0.006 \pm 0.003$ | $0.004 \pm 0.002$ | $0.300 \pm 0.030$ |
| V | $0.000 \pm 0.000$ | $0.019 \pm 0.008$ | $0.013 \pm 0.006$ | $0.417 \pm 0.147$ |
| X | $0.384 \pm 0.140$ | $0.318 \pm 0.117$ | $0.338 \pm 0.124$ | $0.072 \pm 0.025$ |

This table gives the best estimate for the debiased, diameter-limited fractional abundances and albedos of the ten taxonomic complexes. The $T_J \leqslant 3$ and $T_J > 3$ columns are each normalized to unity. Summing over the taxonomic complexes, the NEOs with $T_J \leqslant 3$ account for 30% of the NEOs, and those with $T_J > 3$ account for 70% in a debiased, diameter-limited sample. Within the $T_J \leqslant 3$ population, the C, D, and X complexes account for 86% of the NEOs. Thus, 25% of NEOs are both $T_J \leqslant 3$ and in a dark spectral complex and thus candidates for being extinct comet nuclei. These numbers are represented graphically in Figs. 1–4. These results differ slightly from those of Table 4.7 of Stuart (2003) due to the minor changes in the underlying albedo measurements of Table 2.

(1) Assume that each taxonomic complex follows the binned, non-cumulative absolute magnitude distribution.
(2) For each complex, use the debiased, average albedo and fractional complex abundance, from Table 4 to convert the absolute magnitude distribution to a binned, non-cumulative diameter distribution. This is done by using Eq. (1) to convert the absolute magnitude of each bin to a diameter, and to use the fractional abundances to scale the number of NEOs in the bin to the proper number of NEOs for each complex. This produces 20 separate binned diameter distributions, one for each taxonomic complex, with the $T_J \leqslant 3$ and $T_J > 3$ groups separated as well.
(3) Sort all of these bins from all 20 diameter distributions in order from largest to smallest diameter, and then create a cumulative sum.

The resulting cumulative diameter distribution is shown in Fig. 5.

This final cumulative diameter distribution for the NEOs suffers from at least two problems. One problem is minor, the other is unavoidable. The first problem is that the analysis leading to the average albedos and the debiased fractional

abundances for the complexes assumed an exponential form for the number of NEOs as a function of absolute magnitude. The real absolute magnitude distribution was then added back in at the end of the analysis to obtain a diameter distribution. A more rigorous approach would be to use the full absolute magnitude distribution from the beginning. However, this would eliminate the possibility of using the magnitude-limited debiasing equations (6) and (8), because the derivation of those equations requires an analytical form for the absolute magnitude distribution. In the absolute magnitude range where most of the NEOs with measured albedos reside ($14.5 < H < 18$) the distribution is very close to exponential (Stuart, 2001). Including the full absolute magnitude distribution in the calculations of the observational bias is not warranted because it would be a minor effect on the bias correction factors and the resulting debiased fractional abundances and average albedos. This more complicated approach would also suffer from the second, unavoidable problem.

The second problem with using the binned, non-cumulative absolute magnitude distribution along with the debiased fractional abundances and average albedos to generate a diameter distribution is that it reverses the proper causal order. Using this method makes the assumption that all of the taxonomic complexes have the same absolute magnitude distribution with its various bumps and wiggles lined up at the same place in absolute magnitude. Those bumps and wiggles then get shifted when the absolute magnitude distribution is converted to a diameter distribution for each taxonomic complex. When the diameter distributions for the complexes are summed to obtain the cumulative diameter distribution, the bumps and wiggles that were all lined up in absolute magnitude space get averaged out in diameter space. This is very unlikely to be the case in the real world. The more likely scenario is that the taxonomic complexes have differently shaped diameter distributions reflecting differences in material properties. Any bumps and wiggles in the diameter distribution would get smoothed out when converting to an absolute magnitude distribution. The absolute magnitude distributions for the different taxonomic complexes are very unlikely to be perfectly aligned. However, there is really no alternative to making this assumption. Every NEO that has been discovered has a measured absolute magnitude, whereas only about 3% of them have measured diameters. The absolute magnitude distribution is better constrained than the diameter distribution. Until the albedos and diameters of nearly all of the NEOs have been measured, the best estimate of the diameter distribution will have to be based on the absolute magnitude distribution.

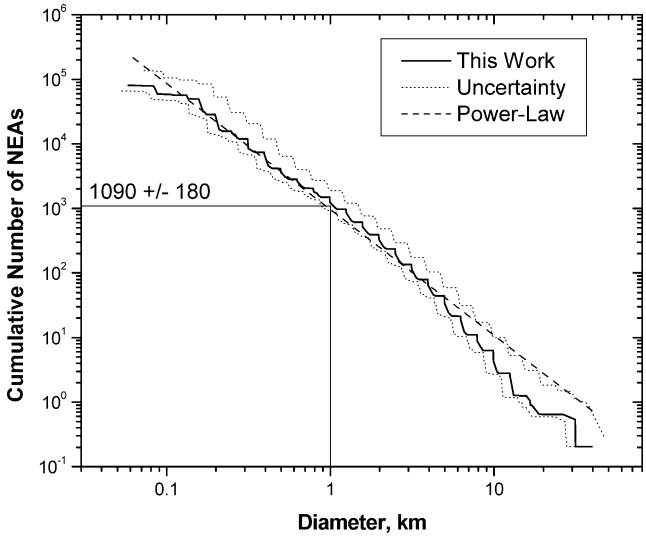


Fig. 5. Cumulative diameter distribution. The solid line shows the cumulative number of NEOs larger than a given diameter. The absolute magnitude distribution (Stuart, 2001) is converted to a diameter distribution using the albedos and fractional abundances for the taxonomic complexes from Table 4. The dotted lines represent an approximate error envelope. The upper side of the error envelope is computed by allowing the number of NEOs in each absolute magnitude bin to be one standard deviation above the best estimate for that bin, and allowing the albedo of each taxonomic complex to be one standard deviation lower than the best estimate for that complex and following the same procedure used to calculate the central red curve (described in the text). The lower side of the error envelope is similarly calculated by allowing the number of NEOs in each $H$ bin to be one standard deviation low, and the albedo of each taxonomic complex to be one standard deviation high. Since the two sources of error are not added in quadrature, the error envelope is somewhat larger than one standard deviation. The straight dashed line is not a fit to the solid curve, but is the power-law distribution derived by assuming an exponential absolute magnitude distribution. The dashed line has a power-law slope ($\alpha$ from Eq. (3)) of $-1.95$, and calibrated with 991 NEOs larger than 1 km, as in Table 3. The number of NEOs with diameters larger than 1 km is $1090 \pm 180$.

Accurate photometry for a large number of main-belt asteroids has recently become available from the Sloan Digital Sky Survey (SDSS) (Jurić et al., 2002). These results indicate that there is a 0.2 magnitude bias in the asteroid catalog of the Minor Planet Center. In its simplest form, the result implies a shift in the absolute magnitudes of all asteroids making them slightly fainter. Consequently, this would result in a reduction in the estimate of the number of NEOs (and main-belt asteroids) at all absolute magnitudes and sizes. Preliminary investigation with the first data release (ADR1.dat) of the Sloan Digital Sky Survey Moving Object Catalog (http://www.astro.princeton.edu/~ivezic/sdssmoc/sdssmoc.html) indicates that the bias is not a simple offset, but rather is dependent on the apparent magnitude, with the offset becoming larger with fainter apparent magnitudes. Only a small number of NEO observations are included in the SDSSMOC (25 observations of 20 different NEOs). The error between the apparent visual magnitude predicted from the cataloged $H$ magnitude and the SDSS measured apparent magnitude (V band synthesized from $r^*$ and $g^*$ bands) is only 0.05 magnitudes, significantly better than the 0.2 magnitude offset found for main-belt asteroids. Properly correcting for photometric bias in the asteroid catalogs is a large task that will not be attempted here. However, the potential exists that all asteroid population estimates may need to be revised downward.

The cumulative diameter distribution shown in Fig. 5 represents the best current estimate of the overall diameter

distribution for the NEOs. In the absolute magnitude distribution used to make the diameter distribution, the bin with the largest absolute magnitude was $H = 22.5$. For the complex with the lowest albedo, (D-types with albedo of 0.042) that absolute magnitude bin corresponds to a diameter of 0.18 km. Below that size, the diameter distribution shown in Fig. 5 is artificially incomplete because of the truncation of the absolute magnitude distribution. This method of computing the diameter distribution gives a slightly higher estimate for the number of NEOs larger 1 km than the estimate given in Table 3. The cumulative diameter distribution pegs the number of NEOs with diameters larger than 1 km at $1090 \pm 180$.

## 2. Impact hazards

With a new model of the orbital distribution and sizes of the NEOs, it is useful to revisit the issue of asteroid impacts on the Earth and Moon. This issue has been addressed many times in the last few decades (Shoemaker et al., 1990; Morrison, 1992; Morbidelli et al., 2002). However, the answer is dependent upon the model one chooses for the NEO population. A new model of the NEO population warrants a new analysis of the NEO impact threat. Furthermore, the ability to predict the lunar crater record, under the assumption of a steady-state population of NEOs, is a critical test for a new NEO population model. The analysis proceeds in three major steps. Step one is to analyze the probability of impact for NEOs into the Earth or Moon. This step depends upon the orbital element distribution of the NEO population, and when combined with the size distribution yields estimates of the frequency of impacts as a function of impactor diameter, or impact energy. The second step is to determine the sizes of craters produced by impactors with specific parameters and to combine this with the impact probabilities to obtain the expected rate of production of craters of various sizes. The third step is to determine how many craters have already been made on the Earth and Moon and to compare this historical cratering record with the predicted rate of crater formation from the current NEO population.

### 2.1. Impact probability calculations

We use Greenberg's method (Greenberg, 1982), with the correction noted by Bottke and Greenberg (1993), to calculate the collision probabilities and collision velocities of NEOs into the Earth and the Moon as detailed in (Stuart, 2003, Chapter 5). The calculations of collision probability for a test asteroid into the Earth or Moon also produce the impact velocities. The velocity is necessary to calculate impact energy and to estimate crater diameter, discussed below. When the calculated impact velocities are weighted by the impact probability, and by the NEO population model, the root-mean-square impact velocity for NEOs hitting the Earth is 20.9 km/s. For that impact velocity, the gravitational capture radius of the Earth is 7540 km, as opposed to the Earth's equatorial radius which is 6378 km. The root-mean-square impact velocity for the Moon is 19.2 km/s, and the corresponding gravitational capture radius is 1751 km, compared to 1738 km for its geometric radius.

When these impact probability calculations are averaged over the NEO orbital element distribution from Stuart (2001), the average impact probability into the Earth is $1.50 \times 10^{-9}$ yr$^{-1}$ per NEO. Morrison et al. (2002) have also calculated the average impact probability, but with a different method. They used the 244 NEOs with absolute magnitudes less than 18 and perihelion distances less than 1.0 AU (i.e., those that cross the Earth's orbit) that had been discovered as of July 3, 2001 to represent the NEO orbital element distribution. The orbits of those 244 NEOs were propagated for 100 yr and all approaches to within 0.1 AU of the Earth were recorded. The encounter velocity of each approach was used to determine the Earth's gravitational capture cross-section for that encounter. The number of encounters was then scaled by the ratio of the gravitational capture cross-sectional area to the cross-sectional area of the study sphere (0.1 AU radius). Morrison et al. found that the impact probability is $1.68 \times 10^{-9}$ yr$^{-1}$ per NEO and that the weighted, RMS impact velocity is 20.2 km/s. Alan Harris (personal communication, 2003) has updated those calculations with more NEOs (thanks to ongoing discoveries), and a longer integration time (1000 yr). The updated impact probability is $1.56 \times 10^{-9}$ yr$^{-1}$ per NEO, with a mean impact velocity of 20.9 km/s. Thus, the semi-analytical methods used in this work, agree nearly perfectly with purely numerical methods using known large NEOs.

We do not use average impact probabilities and velocities to calculate impact rates to the Earth and Moon. Instead the distribution of NEOs as a function of orbital parameters (Stuart, 2001) is combined with the impact probability calculations which are also a function of orbital parameters. The NEOs with $T_J \leqslant 3$ have different collision probabilities, collision velocities, albedo distributions, and density distributions compared to the NEOs with $T_J > 3$. All of those factors are taken into account in this collision model.

### 2.2. Reassessing the Earth impact hazard

Figures 6 and 7 show the cumulative collision probability for the Earth and Moon as a function of absolute magnitude and diameter, using the NEO population model from Stuart (2001), and the diameter distribution derived here. The overall collision hazard for the Earth for asteroids with absolute magnitudes less than 18 is $1.8^{+0.5}_{-0.2} \times 10^{-6}$ yr$^{-1}$, which translates to an average of 1 impact every $0.54^{+0.06}_{-0.1}$ Myr. In terms of impactor diameter, the collision hazard for the Earth is that impacts of 1 km or larger have a probability of $1.67^{+0.4}_{-0.3} \times 10^{-6}$ yr$^{-1}$, or 1 impact every $0.60 \pm 0.1$ Myr.

The real determinant of the damage from an asteroid impact is the total impact energy. In order to calculate the impact energy, one must know the mass of the asteroid, not the diameter. Converting from diameter to mass re-

quires knowledge of the bulk density (and for better accuracy, a complete shape model, rather than just a diameter). The densities of asteroids are even less well sampled than their diameters. However, for C-type and S-type asteroids, there does appear to be a fairly consistent trend (Britt et al., 2002). C-type asteroids have bulk densities clustered around 1400 kg/m$^3$, whereas S-type asteroids have bulk densities clustered around 2700 kg/m$^3$. This agrees with the broad understanding of asteroid formation and mineralogy: C-types formed further out in the asteroid belt of lighter, fluffier material, and S-types formed at higher temperatures on the inner edge of the asteroid belt and are made of rockier material. Individual asteroids could have bulk densities as high as 8000 kg/m$^3$ if they have high metal content, or much lower if they have high internal porosity as result of being a loosely bound accumulation of boulders. The bulk densities of taxonomic categories other than S-types and C-types are entirely unconstrained by actual measurements. Britt et al. (2002) list density measurements for one V-type, one P-type, two M-types, one F-type, and one G-type asteroids. Those are all large main-belt asteroids that may have very different internal porosities than NEOs. In the absence of more density measurements we assume that all of the "dark" taxonomic types (C, D, X) have bulk densities of 1400 kg/m$^3$, and that all of the "bright" types (A, O, Q, R, S, U, V) have densities of 2700 kg/m$^3$. At about 200 m, asteroids probably change from being gravitationally bound rubble piles to being monoliths (Pravec and Harris, 2000; Whiteley et al., 2002). Since a rubble pile has more internal porosity than a monolith, asteroids smaller than 200 m may have substantially higher densities than large asteroids. Most of the results presented here concern large asteroids, and there are no density measurements for asteroids smaller than 200 m, therefore, we have assumed that the bimodal density distribution applies at all sizes.

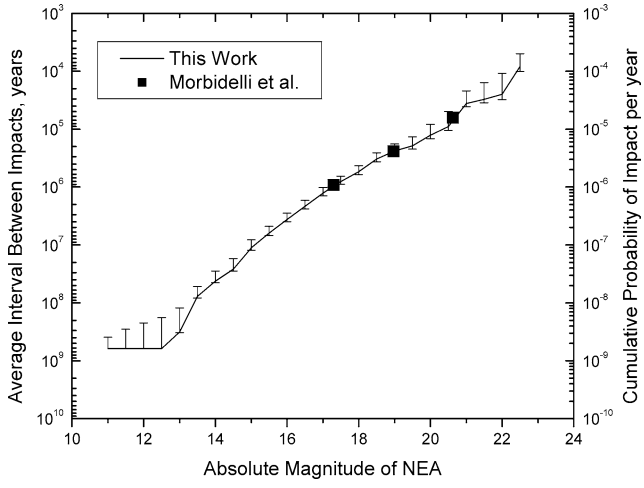


Fig. 6. Probability of NEO Earth impact versus absolute magnitude. The distribution of orbital elements and absolute magnitudes for the NEOs (Stuart, 2001) is combined with impact probability calculations to obtain the cumulative probability of Earth impact for NEOs brighter than a specified absolute magnitude.

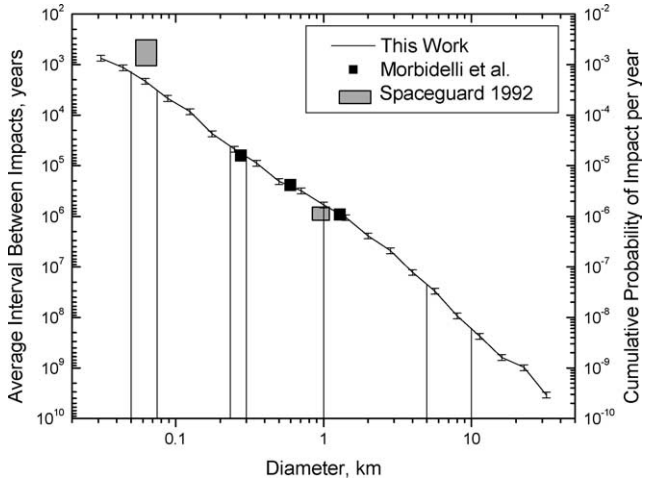


Fig. 7. Probability of NEO Earth impact versus diameter. The distribution of orbital elements for the NEOs (Stuart, 2001) is combined with the debiased diameter distribution derived here, and impact probability calculations to obtain the cumulative probability of Earth impact for NEOs larger than a specified diameter. For comparison, the estimates from Morbidelli et al. (2002) and the Spaceguard Survey Report (Morrison, 1992) are shown. The uncertainties quoted by Morbidelli et al. (2002) are smaller than the plot symbols, while the size of the boxes represent approximate uncertainties for the Spaceguard Report.

Using that density assumption, and the fractional abundances of the taxonomic types from Table 4, the probability of collision can be calculated as a function of impact energy, shown in Fig. 8. The absolute magnitude distribution from Stuart (2001) ends at $H = 22.5$, which corresponds to a diameter of approximately 180 m for the darkest of the taxonomic complexes, the D-types. That absolute magnitude distribution was extended to $H = 25$ in order to estimate the impact rate of bolides with energies as low as that of the Tunguska impactor. This extrapolation was performed by using the power-law fit found in Stuart (2001), $N(< H) = 10^{-3.88+0.39H}$, for $23 \leqslant H \leqslant 25$. The steep falloff in the probability at the largest energies results from a lack of NEOs large enough to produce more energetic impacts.

A recent report by a task force of the government of the United Kingdom of Great Britain (UK NEO Task Force, 2000) focused on impacts larger than $4 \times 10^{18}$ J as being the most significant threat to humanity. These would be from impactor diameters of about 200 m or larger. We find that impacts of that energy or larger have an average impact rate of once every $47{,}000 \pm 6000$ yr. Recent estimates of this value range from $63{,}000 \pm 8000$ yr (Morbidelli et al., 2002) to approximately once every 15,000 yr (Morrison, 1992). The differences in these estimates are due almost entirely to differences in the estimates of the number of NEOs larger than 200 m. These values represent the average time between impacts, but actual impacts could occur more or less closely spaced solely by chance.

The Tunguska event that devastated a region of Siberian forest in 1908 is estimated to have delivered 4–8 $\times 10^{16}$ J

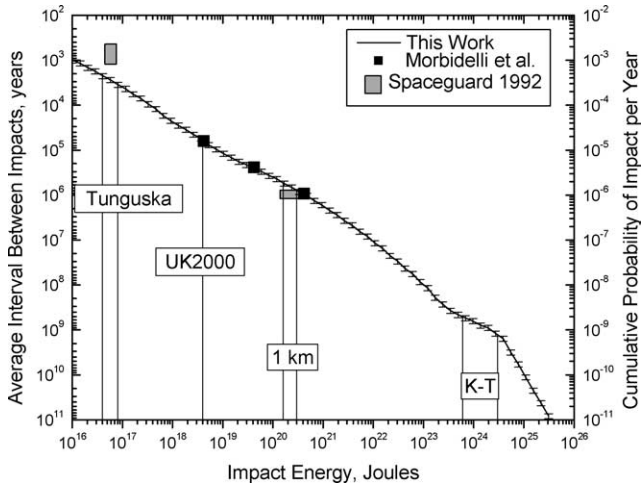


Fig. 8. Probability of NEO impact versus impact energy. The distribution of orbital elements for the NEOs (Stuart, 2001) is combined with the debiased diameter distribution derived here, impact probability calculations, and a bimodal density distribution to obtain the cumulative probability of impact for NEOs with impact energy greater than a given energy. Uncertainties shown represent uncertainty in the number of NEOs but do not reflect uncertainty in their densities. For comparison, 1 megaton of TNT equals $4.18 \times 10^{15}$ J. Vertical lines represent the energy or possible range of energies for various events. The energy from the Tunguska event is estimated as 4–8 $\times 10^{16}$ J (Sekanina, 1998). The UK NEO Task Force identified $4 \times 10^{18}$ J as a threshold for large-scale regional destruction (UK NEO Task Force, 2000). Impact by a 1 km diameter asteroid at the RMS, Earth-impact velocity of 20.9 km/s with a density of 1400 kg/m$^3$ or 2700 kg/m$^3$ would deliver an energy of $1.6 \times 10^{20}$ or $6 \times 10^{20}$ J, respectively. The energy of the K–T impact event that formed the Chicxulub crater is estimated as $6 \times 10^{23}$–$3 \times 10^{24}$ J (Pope et al., 1997). For comparison, the estimates from Morbidelli et al. (2002) and the Spaceguard Survey Report (Morrison, 1992) are shown. The uncertainties quoted by Morbidelli et al. (2002) are smaller than the plot symbols, while the size of the boxes represent approximate uncertainties for the Spaceguard Report.

of kinetic energy with $5 \times 10^{16}$ J being the most likely value (Sekanina, 1998). This range of energies corresponds to an event with a mean interval between impacts of 2000–3000 yr, using the impact frequencies derived here and shown in Fig. 8. However, some researchers have suggested, based on an analysis of the Shoemaker–Levy 9 impacts into Jupiter, that the Tunguska energy could have been as low as $1 \times 10^{16}$ J (Boslough and Crawford, 1997). If this is the correct energy for the Tunguska event, then these events could have a mean interval between impacts as low as 1000 yr. This estimate uses an extrapolation of the exponential fit to the number of NEOs versus absolute magnitude, and so it does not account for deviations from that simple function that might occur in the population of small NEOs. Harris (2002) and Morrison et al. (2002) estimated the frequency of Tunguska-type impactors as once every 1000–3000 yr. That estimate assumes that the average albedo of NEOs is 0.11, somewhat darker than the value of 0.14 found here. They also assumed a mean density of asteroids of 2500 kg/m$^3$, which is higher than the 2050 kg/m$^3$ used here (2050 kg/m$^3$ is an impact probability-weighted average, that is the average density when 2700 kg/m$^3$ for bright complexes and 1400 kg/m$^3$ for dark complexes are averaged after being weighted by the taxonomic abundances in Table 4 and by impact probabilities for NEOs with $T_J \leqslant 3$ or $T_J > 3$). Thus, the estimate by Harris and Morrison et al. of the number of Tunguska-type impactors and the frequency of Tunguska-type events is higher than the estimate given here because of the different values for NEO albedo and density.

To test the potential effect of high bulk densities for small NEOs (as suggested by their rapid rotations) an alternate density assumption was tried. NEOs with diameters smaller than 200 m were assumed to have no porosity, so their bulk densities were increased to the grain densities of presumed meteorite analogs. For the dark complexes, the grain density of CM meteorites (2700 kg/m$^3$) was used. For the bright complexes, the grain density of ordinary chondrite meteorites (3800 kg/m$^3$) was used (Britt et al., 2002). These higher densities among small NEOs results in the average interval between Tunguska-type events being reduced to 1500–2000 yr.

### 2.3. Cratering dynamics

To compare the rate of crater formation expected from the NEO population derived here with the observed craters on the Earth and on the Moon, we will use three crater scaling laws: Melosh's Pi-scaling (Melosh, 1989), Shoemaker's formula (Shoemaker et al., 1990), and Pierazzo's formula (Pierazzo et al., 1997). These are defined briefly in (Stuart, 2003, Chapter 5), and more fully in the references given. The crater scaling formula from Shoemaker et al. (1990) produces the best match between the NEO population and the observed craters.

Since the Shoemaker crater scaling formula (Shoemaker et al., 1990) may be difficult to obtain. We define it here, converting Shoemaker's units to SI mks units:

$$D_t = 0.01436 \left( W \frac{\rho_i}{\rho_t} \right)^{1/3.4} \left( \frac{g_e}{g_t} \right)^{1/6} (\sin \alpha)^{2/3}, \tag{10}$$

where $D_t$ is the transient crater diameter, $W$ is the kinetic energy of the impactor, $\rho_i$ and $\rho_t$ are the bulk densities of the impactor and target respectively, $g_e$ and $g_t$ are the surface accelerations due to gravity of the Earth and the target body respectively, and $\alpha$ is the impact angle (vertical impact has $\alpha = \pi/2$). This formulation is quite similar to Melosh's yield scaling, but without the correction for the penetration depth, and with slightly different treatment of the impactor and target densities. The Shoemaker paper in which this relation is defined treates the results of Eq. (10) as the final, rim-to-rim crater diameter. However, the results are much more consistent with other scaling laws and with the NEO population if Eq. (10) is treated as the transient crater diameter and an additional factor of 1.56 (Melosh, 1989) is used to convert transient crater diameter to final, rim-to-rim crater diameter, $D_r$, as is done in this paper.

Another issue for crater scaling laws is the transition from simple to complex craters, which increases the final crater

size. Shoemaker et al. (1990) uses a simple factor of 1.3 to scale from initial diameters to final, complex crater diameters, and they apply this factor above a transition threshold of $D_* = 4$ km on Earth, with $D_*$ scaling inversely with gravity. Here we use a slightly more complex formula due to Croft (1985):

$$D_f = \frac{D_r^{1.18}}{D_*^{0.18}}. \tag{11}$$

So, to wrap these all together the crater scaling formula that is used here (labeled as Shoemaker in Figs. 9 and 10) is as follows:

$$D_t = 0.01436\left(W\frac{\rho_i}{\rho_t}\right)^{1/3.4}\left(\frac{g_e}{g_t}\right)^{1/6}(\sin\alpha)^{2/3},$$

$$D_r = 1.56 D_t,$$

$$D_f = \begin{cases} D_r & \text{if } D_r \leqslant D_*, \\ \dfrac{D_r^{1.18}}{D_*^{0.18}} & \text{if } D_r > D_*, \end{cases}$$

$$D_* = 4\,\text{km}\left(\frac{g_e}{g_t}\right), \tag{12}$$

where all units are mks, $D_t$, $D_r$, $D_f$ refer to transient, rim-to-rim, and final crater diameters respectively, $\rho$ and $g$ are density and surface acceleration due to gravity with subscripts $i$, $t$, $e$ indicating impactor, target, and Earth, respectively, and $\alpha$ is the impact angle (vertical impact has $\alpha = \pi/2$).

Continuing to use the assumption given above that dark NEOs (C, D, X complexes) have bulk densities of 1400 kg/m$^3$ and that bright NEOs (S, Q, etc. complexes) have bulk densities of 2700 kg/m$^3$, we can use any of the crater scaling laws to convert the impact rates that are given above as a function of impactor size into crater production rates for craters larger than a specified size, either on the Earth or on the Moon. This rate of crater production represents the current rate of crater production from NEOs. It does not include craters produced by long-period comets. The current rate of crater production, as derived from estimates of the NEO population can be compared with the historical cratering record.

### 2.4. Crater counting on the Moon

The most comprehensive assessment of the post-mare cratering rate is Chapter 8 of the book *Basaltic Volcanism on the Terrestrial Planets* (Hartmann et al., 1981) (henceforth referred to as BVTP). BVTP does not explicitly give uncertainties for their estimated cratering rates but suggest that crater counts by different authors differ by about 30%. Uncertainties in the area in which craters are counted and in the ages of geological provinces would increase the uncertainty in the crater rate to more than 30%. A recent analysis by Stöffler and Ryder (2001), indicates that the ages used in BVTP for the maria are too old by about 4% on average. This correction would increase the BVTP cratering rate

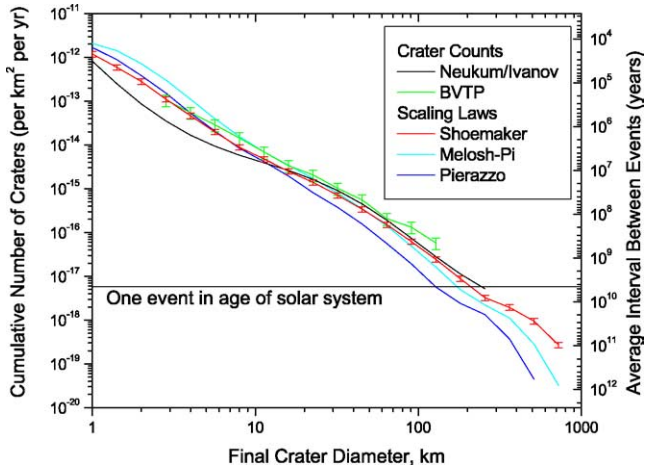


Fig. 9. Lunar cratering rate. The rate of formation of craters on the lunar maria (Ivanov et al., 2001; Hartmann et al., 1981) is compared with the expected rate of crater formation from the NEO population models presented here. The three curves showing the NEO model results use different crater scaling laws to derive crater diameters, but all use the same NEO population model derived here. The uncertainties shown for the preferred model, Shoemaker scaling, are calculated by increasing or decreasing the number of NEOs in the population model by $1\sigma$ (or 180 NEOs at 1 km) and do not include uncertainties in asteroid density or crater scaling laws. The overall rate of lunar crater formation, as derived from the NEO population model with the Shoemaker scaling law, matches the rate predicted by counting craters on the lunar maria (BVTP) over crater diameters from 2 to over 100 km. The lunar crater production function from Neukum and Ivanov is also shown for comparison (Ivanov et al., 2001). This matches quite well with the NEO production function (Shoemaker scaling) for diameters greater than 10 km. However, below 10 km, there is a severe mismatch with the highlands crater production function being a factor of 3 or more lower than the production function based on the NEO population model.

by 4% at all crater diameters. This correction has not been applied here in comparing the BVTP crater production function with the NEO population. The BVTP crater production function used for comparison here has been taken directly from Table 8.4.1 of BVTP. The cumulative crater density of the average of lunar front-side maria is divided by the average age of the returned lunar maria samples, 3.45 Gyr.

More recent presentations of the lunar cratering rate have been made by Neukum, Ivanov, and coauthors (Ivanov et al., 2001; Werner et al., 2002; Neukum and Ivanov, 1994). A primary difference between the crater production function of Neukum et al. and that of BVTP is the inclusion of craters from the older lunar highlands which may have been subjected to a substantially higher cratering rate during the Late Heavy Bombardment (Hartmann et al., 2000). We also compare the lunar crater production function based on the NEO population model to the highlands production function of Neukum and Ivanov.

### 2.5. Comparison with the lunar crater record

Figure 9 shows the BVTP crater production function for the average of front-side lunar maria, and the highlands crater production function of Neukum and Ivanov compared with the current cratering rate as predicted by my popula-

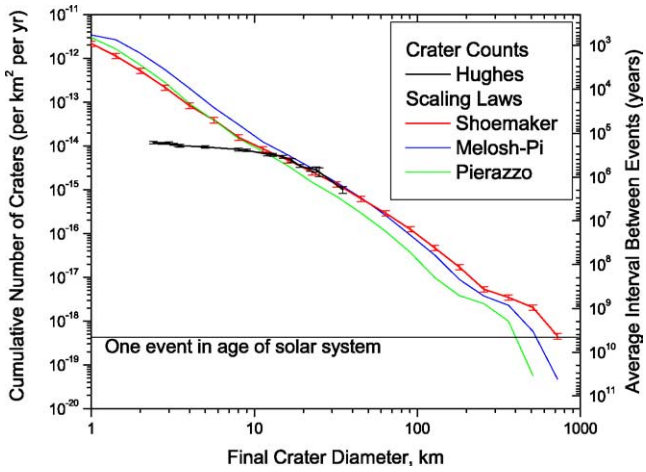


Fig. 10. Terrestrial cratering rate. The rate of production of craters on the Earth as cataloged by Hughes (2000) is compared with the expected rate of crater formation from the impact of NEOs. The NEO population model derived here is combined with three crater scaling laws to estimate the current crater production function on the Earth. The preferred scaling law (Shoemaker) is shown with uncertainties computed by changing the number of NEOs in the population model by 1 standard deviation, and do not include uncertainties in NEO density or crater scaling laws. The NEO population model combined with either the Shoemaker or Melosh-Pi scaling laws matches the crater production function determined from counting craters on the Earth in the size range from 15 to 35 km (Hughes, 2000). Below 15 km, craters on the Earth are eroded by weather and so the counts of small craters are severely depleted.

tion model and various crater scaling laws. The predicted crater production function from the NEO population model is quite similar to the function derived by counting craters on the lunar maria. This is consistent with the NEO population being in steady-state, and with the rate of lunar crater production being constant for the last 3 Gyr. It also agrees with other recent analyses of the rate of comet impacts and suggests that comet impacts are a minor contributor to the total impactor flux (Weissman et al., 2002). The crater production function of Neukum and Ivanov matches the crater production function derived from the NEO population for crater diameters larger than 10 km. However, there is a significant mismatch in the range of 1 to 10 km. The largest difference is that the Neukum/Ivanov production function is a factor of 7 lower than the NEO production function at crater diameters of 2.8 km.

Werner et al. (2002) performed a similar comparison between the Neukum/Ivanov lunar crater production function, and the NEO population estimates of D'Abramo et al. (2001) and Rabinowitz et al. (2000). They performed the calculations in the opposite direction, converting the lunar crater production function into a impactor size-frequency distribution. This approach has the disadvantage that it must use an average impact velocity and impactor density. It cannot use a distribution of impact velocities or a distribution of impactor densities, as was done here, because there is no way to estimate those quantities from an observed crater. Werner et al. found reasonably good agreement between the Neukum/Ivanov crater production function and the NEO population estimates of D'Abramo et al. and Rabinowitz et al. Those two NEO population estimates are lower than the NEO population estimate derived here. The Neukum/Ivanov crater production function is also lower than the BVTP crater production function for crater diameters from $\sim 3$ to $\sim 15$ km.

### 2.6. Comparison with the terrestrial crater record

Geologic processes of erosion and plate subduction make calculations of cratering rates on the Earth much more problematic than on the Moon. Small craters on the Earth are erased quickly, very little of the Earth's crust is old enough to have accumulated enough large craters to count, and much of the Earth is covered by oceans in which craters last only a few minutes. However, the craters that are observed on the Earth are available for close scrutiny. Accurate ages can be obtained for each crater, and the crater rim and floor can be studied to characterize slumping and formation of complex crater features such as central uplifts. The cratering record on the Earth has been studied extensively in the last few decades, especially since the Cretaceous–Tertiary extinction event was linked with an impact (Alvarez et al., 1980). Figure 10 shows the rate of production of impact craters on the Earth (Hughes, 2000) as determined by counting and dating impact structures, compared to the rate predicted from the NEO population. We have assumed a density of 2700 kg/m$^3$ for terrestrial target rocks. As with the lunar crater production predictions, the sharp turnover in the predicted number of large craters on the Earth is because of a lack of NEOs large enough to produce such large craters. On the Earth, however, the reduction in the number of very small craters, less than about 1 km diameter, is probably real. The simulation included NEOs down to 50 m in diameter. At sizes below 50 m, the atmosphere shields the surface of the Earth from impact.

Above crater sizes of about 15 km, the observed cratering rate on the Earth matches the rate predicted from the NEO population models. Below 10 km, there is a pronounced deficit of observed craters. Most researchers (Grieve and Shoemaker, 1994, for example) attribute the deficit of small craters to erosion that erases them from the crater record, and assume that, in the absence of erosion, the production rate of craters should continue upward roughly as a power law. Hughes (2000), however, argues that the deficit of small craters is a real feature of the rate of production of craters, and not due to some size-dependent erosional process. It is impossible to reconcile that view with observational data of NEOs. A deficit of craters in the 10 km range would require a sharp deviation from a power law in the number of NEOs starting at sizes around 1 km. This marked reduction in the number of 1 km NEOs is not observed. It is also impossible to reconcile this deficit of craters smaller than 10 km with the cratering record on the Moon which is consistent with the cratering rate deduced from the observed population of NEOs down to crater sizes of 2 km.

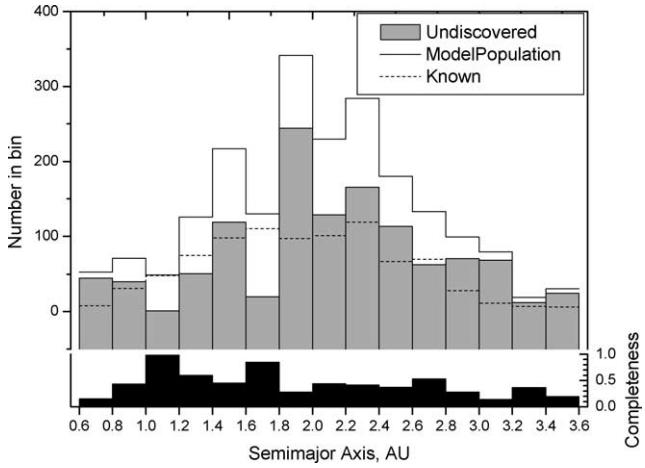


Fig. 11. Semimajor axis distribution of NEOs. The population model of Stuart (2001) is compared with the known population as of 2003 November 7. The undiscovered population is the difference, in each semimajor axis bin, between the model population and the known population. The bottom panel gives the completeness in each bin, or the fraction of the model population that has already been discovered.

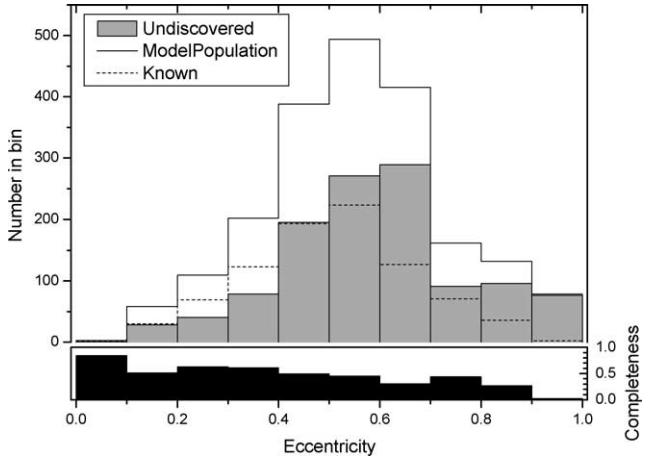


Fig. 12. Eccentricity distribution of NEOs. The population model of Stuart (2001) is compared with the known population as of 2003 November 7. The undiscovered population is the difference, in each eccentricity bin, between the model population and the known population. The bottom panel gives the completeness in each bin, or the fraction of the model population that has already been discovered.

### 2.7. *Undiscovered NEOs*

Now that the worldwide effort to catalog NEOs has found more than half of the objects larger than 1 km, it is useful to see how the NEOs that have been discovered already compare with those still undiscovered in terms of orbital element distributions. Of course, the orbital elements of undiscovered NEOs are not known, but a debiased population model can be used to estimate the properties of the NEOs that have not been found. In Figs. 11–13 we compare a debiased population model (Stuart, 2001, 2003) with known population as of 2003 November 7. For both the model population and the known population, NEOs with absolute magnitude brighter than 18.5 are included, and the four-dimensional parameter

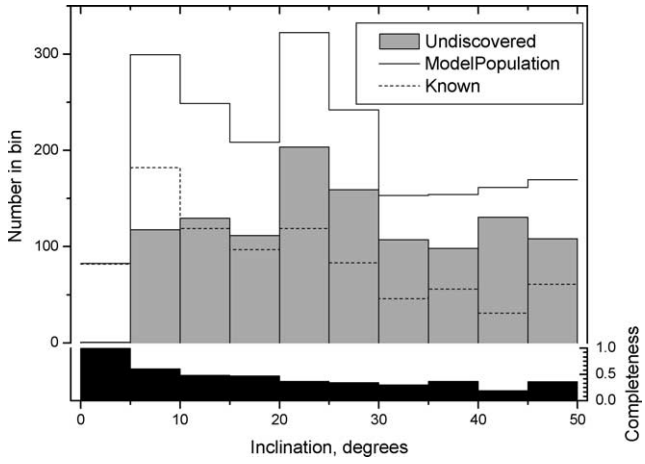


Fig. 13. Inclination distribution of NEOs. The population model of Stuart (2001) is compared with the known population as of 2003 November 7. The undiscovered population is the difference, in each inclination bin, between the model population and the known population. The bottom panel gives the completeness in each bin, or the fraction of the model population that has already been discovered.

space is collapsed into three one-dimensional histograms by summing over the other three dimensions. The "undiscovered" population is the difference between the model population and the known population in each bin. Also shown are the completeness fractions in each bin, or the fraction of the model population that has already been discovered.

## 3. Conclusions

We have presented the results of debiasing the measured albedos of the NEOs. The debiasing technique uses an averaging algorithm that ensures that the number of NEOs bigger than a given size will be the same as the number of NEOs brighter than the equivalent absolute magnitude limit when the resulting average albedo is used to convert between diameter and absolute magnitude. For the purpose of counting asteroids, this type of average is an improvement over the geometric mean.

The average albedos for the taxonomic complexes come out being similar to the main belt but generally a little bit higher than the main-belt averages. Table 5 summarizes this for the three complexes for which there are an appreciable number of both main-belt asteroid (MBA) and NEO albedos available. For the C-types, the NEOs are nearly twice as reflective as their main-belt counterparts, while the S-type NEOs are only slightly brighter, and the X-types are slightly darker. This higher reflectance for the C-types is a surprising result that could be due to some residual bias against the discovery of lower albedo C-types relative to higher albedo C-types.

The debiased fractional abundances of the NEOs do not match with the debiased fractional abundances of large MBAs (diameters $\geqslant$ 20 km). Bus and Binzel (2002b) present, in their Fig. 19, debiased fractional abundances of the taxo-

Table 5
Comparison of main-belt and NEO albedos

| Taxonomic complex | Main-belt albedo | NEO albedo |
|---|---|---|
| C | $0.06 \pm 0.04$ | $0.101 \pm 0.027$ |
| S | $0.20 \pm 0.06$ | $0.238 \pm 0.044$ |
| X | $0.10 \pm 0.09$ | $0.072 \pm 0.025$ |

The albedos for the main belt are as defined in footnote 1. The albedos for the NEOs are the debiased average albedos for the complex as in Fig. 1. The debiased albedos for the S and X complexes are indistinguishable from the average main-belt values, however the C-type NEOs are somewhat brighter than their main-belt counterparts.

nomic complexes within the main belt. The fractional abundances for the NEOs presented here do not match very well with the abundances for the MBAs. This is not surprising, as the NEOs are not necessarily a representative sample of the main belt. Bottke et al. (2002), for example, show a higher probability for NEO delivery through the $\nu_6$ resonance. Relatively recent collisions near the resonance could lead to abundances of particular types of asteroids in the current NEO population. Indeed, the taxonomic abundances of the NEO population may be the best way to reconstruct the spectral characteristics of the small asteroids that feed the resonance zones, if the NEOs can be traced back to their origins in the main belt. As discussed in Binzel et al. (2004) taxonomic signatures of the source regions are measurable in the NEO population. With more spectral and albedo measurements of NEOs, the distributions of taxonomic types of the small main-belt asteroids feeding the source regions should begin to emerge.

The debiasing procedure we used assumed that there was no correlation between the albedos (or spectra) and the orbital parameters or size, other than the trend produced by the Tisserand parameter. While some suggested trends are emerging with respect to size (Delbo et al., 2003; Binzel et al., 2004), only with a substantial increase in the quantity of spectral and albedo data will it be possible to model these additional dependencies in an analysis of the debiased NEO population.

The X-types form a substantial fraction of the NEOs. As can be seen in Fig. 3, the relatively low average albedo of the X-types significantly boosts their fractional abundance after debiasing. Since the albedos of the X-types span a large range (from 0.023 to 0.55) the debiased albedo for the complex is particularly dependent upon the small number of measurements of very dark objects. However, the resulting average albedo ($0.072 \pm 0.025$) is similar to values for the main-belt X-types, so the debiasing technique is producing a reasonable estimate for the average NEO albedos. It would be useful to obtain more albedo measurements of the X-type NEOs to further refine this average.

If we combine the taxonomic complexes into two groups (complexes A, O, Q, R, S, U, and V become the bright group, and C, D, and X become the dark group), the bright objects account for 38% of the NEOs, and the dark objects account for 62% in a diameter-limited sample. This produces a dark:bright ratio of 1.60. Other researchers recently found a different dark:bright ratio of 0.87 among the NEOs (Morbidelli et al., 2002). The dark:bright ratio presented here includes the large (33% of NEO population) contribution of the X-types among the dark part of the NEO population because their average albedo is 0.072. Morbidelli et al. did not explicitly model the taxonomic complexes, but the treatment of the abundant X-types may be the cause of the discrepancy between these two dark:bright ratios. Apart from the difference between the dark:bright ratios, the Morbidelli et al. model agrees very well with the results found here. Morbidelli et al. find that the absolute magnitude threshold that corresponds to a 1 km diameter NEO is 17.85, or an average albedo 0.13. That value is similar to the value found here ($0.139 \pm 0.02$). The impact rates as a function of impact energy derived by Morbidelli et al. also agree closely with the rates found here (Fig. 8).

We have presented an average albedo for the NEOs as a whole so that the estimates of the NEO population that are presented as a function of absolute magnitude may be converted to population estimates as a function of diameter. The average albedo is slightly brighter than the generally assumed value of 0.11. Because most recently published estimates of the number of 1 km NEOs assumed the value of 0.11 when converting absolute magnitude to diameter, the estimates for the number of 1 km NEOs has been somewhat high. We have found that there are about 1090 ($\pm$180) NEOs with diameters larger than 1 km. Currently (2004 June), the Minor Planet Center catalog lists 611 known NEOs with absolute magnitudes $H < 17.76$. This implies that the current catalog of known NEOs larger than 1 km in diameter is about 56% complete for NEOs bigger than 1 km.

The model of the NEO population developed here has been used to predict the rate of impacts of NEOs into the Earth and Moon. The Earth suffers globally catastrophic NEO impacts (larger than 1 km diameter impactor) at an average rate of once every 500,000 to 700,000 yr, and regionally devastating impacts ($4 \times 10^{18}$ J or more of impact energy) every 41,000 to 53,000 yr. Impacts with energies near that of the Tunguska impactor occur with an average rate of once every 2000 to 3000 yr. The rate of crater formation on the Earth and Moon, as predicted by the NEO population model combined with a simple NEO density assumption, impact probability estimates, and crater scaling laws, is consistent with the observed number of craters on the Earth and Moon.

These results combine the largest set of NEO discovery statistics from a single survey, the largest set of physical data on NEOs, and corrections for observational bias. The result is a comprehensive estimate of the total NEO population in terms of orbital parameters, absolute magnitudes, albedos, and sizes. This improved description of the NEOs will help us to plan surveys to find and study the remaining undiscovered NEOs, to connect the NEOs to their origins in the main belt, to connect the NEOs to meteorite samples, to compare the Lunar and Terrestrial cratering record to

the current population of potential impactors, and to understand the magnitude of the NEO impact hazard to the Earth's biosphere.

## Acknowledgments

We are grateful to a large number of people who assisted in this work in one way or another including Schelte (Bobby) Bus, Tom Burbine, Andy Rivkin, William Bottke, Alessandro Morbidelli, Frank Shelly, two Alan W. Harrises, and Marco Delbo, and we would like to welcome Heath and Jasper who arrived during proof corrections. J.S.S. received support for this work from the Lincoln Scholars Program at MIT Lincoln Laboratory, by NASA, and by the Department of the Air Force under Air Force Contract F19628-00-C-0002. R.B.P. received supported from the National Science Foundation under Grant No. 0205863 and NASA under Grant NAG5-12355. Opinions, interpretations, conclusions, and recommendations are those of the authors and are not necessarily endorsed by the United States Government.

## References

Alvarez, L.W., Alvarez, W., Asaro, F., Michel, H.V., 1980. Extraterrestrial cause for the cretaceous tertiary extinction. Science 208, 1095–1108.

Bevington, P.R., 1969. Data Reduction and Error Analysis for the Physical Sciences. McGraw–Hill, New York, NY.

Binzel, R.P., Lupishko, D.F., Di Martino, M., Whiteley, R.J., Hahn, G.J., 2002a. Physical properties of near-Earth objects. In: Bottke, W.F., Cellino, A., Paolicchi, P., Binzel, R.P. (Eds.), Asteroids III. Univ. of Arizona Press, Tucson, pp. 251–271.

Binzel, R.P., Rivkin, A.S., Bus, S.J., Delbo, M., Harris, A.W., Harris, A.W., 2002b. Spectral and albedo properties of the near-Earth object population. In: Asteroids, Comets, Meteors 2002. Meeting. Abstract 18-040.

Binzel, R.P., Rivkin, A.S., Stuart, J.S., Harris, A.W., Bus, S.J., Burbine, T.H., 2004. Observed spectral properties of near-Earth objects: results for population distribution, source regions, and space weathering processes. Icarus 170, 259–294.

Boslough, M.B.E., Crawford, D.A., 1997. Shoemaker–Levy 9 and plume-forming collisions on Earth. Ann. NY Acad. Sci. 822, 236–282.

Bottke, W.F., Greenberg, R., 1993. Asteroidal collision probabilities. Geophys. Res. Lett. 20 (10), 879–881.

Bottke, W.F., Jedicke, R., Morbidelli, A., Petit, J., Gladman, B., 2000. Understanding the distribution of near-Earth asteroids. Science 288, 2190–2194.

Bottke, W.F., Morbidelli, A., Jedicke, R., Petit, J., Levison, H.F., Michel, P., Metcalfe, T.S., 2002. Debiased orbital and absolute magnitude distribution of the near-Earth objects. Icarus 156 (2), 399–433.

Britt, D.T., Yeomans, D., Housen, K., Consolmagno, G., 2002. Asteroid density, porosity, and structure. In: Bottke, W.F., Cellino, A., Paolicchi, P., Binzel, R.P. (Eds.), Asteroids III. Univ. of Arizona Press, Tucson, pp. 485–500.

Bus, S.J., 1999. Compositional structure in the asteroid belt: results of a spectroscopic survey. Thesis. Massachusetts Institute of Technology, Cambridge.

Bus, S.J., Binzel, R.P., 2002a. Phase II of the small main-belt asteroid spectroscopic survey: the observations. Icarus 158 (1), 106–145.

Bus, S.J., Binzel, R.P., 2002b. Phase II of the small main-belt asteroid spectroscopic survey: a feature-based taxonomy. Icarus 158 (1), 146–177.

Croft, S.K., 1985. The scaling of complex craters. Proc. Lunar Planet. Sci. Conf. 15th. J. Geophys. Res. 90, C828–C842.

D'Abramo, G., Harris, A.W., Boattini, A., Werner, S.C., Harris, A.W., Valsecchi, G.B., 2001. A simple probabilistic model to estimate the population of near-Earth asteroids. Icarus 153, 214–217.

Delbo, M., Harris, A.W., Binzel, R.P., Pravec, P., Davies, J.K., 2003. Keck observations of near-Earth asteroids in the thermal infrared. Icarus 166, 116–130.

Fernández, Y.R., Jewitt, D.C., Sheppard, S.S., 2001. Low albedos among extinct comet candidates. Astrophys. J. 553, L197–L200.

Fowler, J.W., Chillemi, J.R., 1992. IRAS Asteroid Data Processing. In: The IRAS Minor Planet Survey. Tech. Rep. PL-TR-92-2049. Phillips Laboratory, Hanscom Air Force Base, Massachusetts, pp. 17–43.

Greenberg, R., 1982. Orbital interactions—a new geometrical formalism. Astron. J. 87, 184–195.

Grieve, R.A.F., Shoemaker, E.M., 1994. The record of past impacts on Earth. In: Gehrels, T. (Ed.), Hazards Due to Comets and Asteroids. Univ. of Arizona Press, Tucson, pp. 417–462.

Harris, A.W., 1998. A thermal model for near-Earth asteroids. Icarus 131, 291–301.

Harris, A.W., 2002. A new estimate of the population of small NEAs. American Astronomical Society, DPS meeting #34, #02.02.

Harris, A.W., Davies, J.K., 1999. Physical characteristics of near-Earth asteroids from thermal infrared spectrophotometry. Icarus 142, 464–475.

Harris, A.W., Harris, A.W., 1997. On the revision of radiometric albedos and diameters of asteroids. Icarus 126, 450–454.

Harris, A.W., Lagerros, J.S.V., 2002. Asteroids in the thermal infrared. In: Bottke, W.F., Cellino, A., Paolicchi, P., Binzel, R.P. (Eds.), Asteroids III. Univ. of Arizona Press, Tucson, pp. 205–218.

Harris, A.W., Davies, J.K., Green, S.F., 1998. Thermal infrared spectrophotometry of the near-Earth Asteroids 2100 Ra–Shalom and 1991 EE. Icarus 135, 441–450.

Hartmann, W.K., Strom, R.G., Grieve, R.A.F., Weidenschilling, S.J., Diaz, J., Blasius, K.R., Chapman, C.R., Woronov, A., Shoemaker, E.M., Dence, M.R., Jones, K.L., 1981. Chronology of planetary volcanism by comparative studies of planetary cratering. In: Basaltic Volcanism on the Terrestrial Planets (Basaltic Volcanism Study Project). Pergamon Press, New York, pp. 1049–1129. Chapter 8.

Hartmann, W.K., Ryder, G., Dones, L., Grinspoon, D., 2000. The time-dependent intense bombardment of the primordial Earth/Moon system. In: Canup, R.M., Righter, K. (Eds.), Origin of the Earth and Moon, pp. 493–512.

Howell, E.S., Merenyi, E., Lebofsky, L.A., 1994. Classification of asteroid spectra using a neural network. J. Geophys. Res. 99 (E5), 10847–10865.

Hughes, D.W., 2000. A new approach to the calculation of the cratering rate of the Earth over the last $125 \pm 20$ Myr. Mon. Not. R. Astron. Soc. 317 (2), 429–437.

Ivanov, B.A., Neukum, G., Wagner, R., 2001. Size-frequency distributions of planetary impact craters and asteroids. In: Marov, M.Y., Rickman, H. (Eds.), Collisional Processes in the Solar System. Kluwer, Dordrecht, pp. 1–34.

Jurić, M., 16 colleagues, 2002. Comparison of positions and magnitudes of asteroids observed in the Sloan Digital Sky Survey with those predicted for known asteroids. Astron. J. 124, 1776–1787.

Kresák, L., 1979. Dynamical interrelations among comets and asteroids. In: Gehrels, T. (Ed.), Asteroids. Univ. of Arizona Press, Tucson, pp. 289–309.

Luu, J., Jewitt, D., 1989. On the relative numbers of C types and S types among near-Earth asteroids. Astron. J. 98, 1905–1911.

Melosh, H.J., 1989. Impact cratering: a geologic process. In: Oxford Monographs on Geology and Geophysics, vol. 11. Oxford Univ. Press, Oxford, pp. 1–253.

Morbidelli, A., Jedicke, R., Bottke, W.F., Michel, P., Tedesco, E.F., 2002. From magnitudes to diameters: the albedo distribution of near Earth objects and the Earth collision hazard. Icarus 158 (2), 329–342.

Morrison, D., 1992. The Spaceguard survey: report of the NASA International Near-Earth-Object Detection Workshop. Jet Propulsion Laboratory/California Institute of Technology.

Morrison, D., Harris, A.W., Sommer, G., Chapman, C.R., Carusi, A., 2002. Dealing with the impact hazard. In: Bottke, W.F., Cellino, A., Paolicchi, P., Binzel, R.P. (Eds.), Asteroids III. Univ. of Arizona Press, Tucson, pp. 739–754.

Mottola, S., 28 colleagues, 1997. Physical model of near-Earth Asteroid 6489 Golevka (1991 JX) from optical and infrared observations. Astron. J. 114, 1234.

Neukum, G., Ivanov, B.A., 1994. Crater size distributions and impact probabilities on Earth from lunar, terrestrial-planet, and asteroid cratering data. In: Gehrels, T. (Ed.), Hazards Due to Comets and Asteroids. Univ. of Arizona Press, Tucson, pp. 359–416.

Pope, K.O., Ocampo, A.C., Baines, K.H., 1997. Constraints on volatile production by the Chicxulub impact. In: Proc. Lunar Planet. Sci. Conf. 28th, pp. 127–128.

Pierazzo, E., Vickery, A.M., Melosh, H.J., 1997. A reevaluation of impact melt production. Icarus 127 (2), 408–423.

Pravec, P., Harris, A.W., 2000. Fast and slow rotation of asteroids. Icarus 148 (1), 12–20.

Pravec, P., Wolf, M., Sarounova, L., Harris, A.W., Davies, J.K., 1997. Spin vector, shape, and size of the AMOR Asteroid (6053) 1993 BW_3. Icarus 127 (2), 441–451.

Rabinowitz, D., Helin, E., Lawrence, K., Pravdo, S., 2000. A reduced estimate of the number of kilometer-sized near-Earth asteroids. Nature 403, 165–166.

Russell, H.N., 1916. On the albedo of the planets and their satellites. Astrophys. J. 18 (3), 173–196.

Sekanina, Z., 1998. Evidence for asteroidal origin of the Tunguska object. Planet. Space Sci. 46 (2/3), 191–204.

Shoemaker, E.M., Wolfe, R.F., Shoemaker, C.S., 1990. Asteroid and comet flux in the neighborhood of Earth. Geological Society of America Special Paper 247.

Stöffler, D., Ryder, G., 2001. Stratigraphy and isotope ages of lunar geologic units: chronological standard for the inner Solar System. In: Kallenbach, R., Geiss, J., Hartmann, W.K. (Eds.), Chronology and Evolution of Mars. Kluwer, Dordrecht, pp. 9–54.

Stokes, G.H., Evans, J.B., Viggh, H.E.M., Shelly, F.C., Pearce, E.C., 2000. Lincoln near-Earth asteroid program (LINEAR). Icarus 148 (1), 21–28.

Stuart, J.S., 2001. A near-Earth asteroid population estimate from the LINEAR survey. Science 294, 1691–1693.

Stuart, J.S., 2003. Observational constraints on the number, albedos, sizes, and impact hazards of the near-Earth asteroids. Doctoral thesis. Massachusetts Institute of Technology, Cambridge, Massachusetts.

Tedesco, E.F., Williams, J.G., Matson, D.L., Weeder, G.J., Gradie, J.C., Lebofsky, L.A., 1989. A three-parameter asteroid taxonomy. Astron. J. 97, 580–606.

Tedesco, E.F., Noah, P.V., Noah, M., Price, S.D., 2002. The supplemental IRAS minor planet survey. Astron. J. 123 (2), 1056–1085.

Tholen, D.J., 1984. Asteroid taxonomy from cluster analysis of photometry. Doctoral thesis. The University of Arizona, Tucson, Arizona.

UK NEO Task Force, 2000. Report of the task force on potentially hazardous near Earth objects. UK NEO Information Centre, London. http://www.neareathobjects.co.uk/.

Weissman, P.R., Bottke, W.F., Levison, H.F., 2002. Evolution of comets into asteroids. In: Bottke, W.F., Cellino, A., Paolicchi, P., Binzel, P. (Eds.), Asteroids III. Univ. of Arizona Press, Tucson, pp. 669–686.

Werner, S.C., Harris, A.W., Neukum, G., Ivanov, B.A., 2002. NOTE: the near-Earth asteroid size-frequency distribution: a snapshot of the lunar impactor size-frequency distribution. Icarus 156 (1), 287–290.

Whiteley, R.J., Tholen, D.J., Hergenrother, C.W., 2002. Lightcurve analysis of four new monolithic fast-rotating asteroids. Icarus 157 (1), 139–154.

Xu, S., Binzel, R.P., Burbine, T.H., Bus, S.J., 1995. Small main-belt asteroid spectroscopic survey: initial results. Icarus 115 (1), 1–35.